

Article

Treatment of a Food Industry Dye, Brilliant Blue, at Low Concentration Using a New Photocatalytic Configuration

Fatine Drhimer^{1,2}, Maryem Rahmani¹, Boutaina Regraguy¹, Souad El Hajjaji¹, Jamal Mabrouki^{1,*} , Abdeltif Amrane² , Florence Fourcade² and Aymen Amine Assadi^{2,3} 

¹ Laboratoire de Spectroscopie, Modélisation Moléculaire, Matériaux, Nanomatériaux, Eau et Environnement, Faculté des Sciences, Mohammed V University in Rabat, Av. Ibn Battouta, B.P. 1014, Rabat M-10000, Morocco

² École Nationale Supérieure de Chimie de Rennes, University Rennes, 11, Allée de Beaulieu-CS 50837, CEDEX 07, 35708 Rennes, France

³ College of Engineering, Imam Mohammad Ibn Saud Islamic University, IMSIU, Riyadh 11432, Saudi Arabia

* Correspondence: jamal.mabrouki@um5r.ac.ma

Abstract: Food coloring has become one of the main sources of water pollution. Brilliant blue (BB) is one of the dyes used in the food industry. Heterogeneous photocatalysis is increasingly used to decontaminate polluted water from food industries. The objective of this paper was to treat this pollution using a photoreactor at the laboratory (batch) and pilot scales. The photodegradation of the brilliant blue dye, chosen as a model of pollutant, was performed at room temperature in an aqueous solution of titanium dioxide supported on cellulosic paper in the presence of an external UV lamp. The surface morphology of this photoactive tissue was characterized by SEM and FTIR. The performances of two geometric configurations were examined (batch reactor and annular recirculation reactor) in accordance with degradation and pollutant mineralization. The performance of the photocatalytic system was optimized by a parametric study to improve the impact of the different parameters on the efficiency of the degradation process, namely the initial concentration of the pollutant, the TiO₂ cycle, the pH of the solution with the recirculating reactor, and the flow rate. The results showed 98% degradation of brilliant blue at the laboratory scale and 93.3% and 75% at the pilot flow rates of 800 and 200 L·h⁻¹, respectively. The supported semiconductor showed good photodegradation ability during BB decomposition, showing that photocatalysis is a promising technique for water purification.

Keywords: photocatalysis; food processing discharge; batch reactor; circulating reactor



check for updates

Citation: Drhimer, F.; Rahmani, M.; Regraguy, B.; El Hajjaji, S.; Mabrouki, J.; Amrane, A.; Fourcade, F.; Assadi, A.A. Treatment of a Food Industry Dye, Brilliant Blue, at Low Concentration Using a New Photocatalytic Configuration.

Sustainability **2023**, *15*, 5788.

<https://doi.org/10.3390/su15075788>

su15075788

Academic Editor: Goksel Demirer

Received: 2 February 2023

Revised: 17 March 2023

Accepted: 21 March 2023

Published: 27 March 2023



Copyright: © 2023 by the authors. Licensee MDPI, Basel, Switzerland. This article is an open access article distributed under the terms and conditions of the Creative Commons Attribution (CC BY) license (<https://creativecommons.org/licenses/by/4.0/>).

1. Introduction

The agri-food industry has become a world-leading sector, producing large quantities of highly colored effluents. It is known that the existence of industrial pollutants is an important source of risk in industrial facilities' discharges, especially agri-food discharges, which pose serious problems to humans and the environment [1,2]. Most of these contaminants are undegradable and persistent [3]. They are difficult to remove by traditional coagulation, filtration, or adsorption methods [4–6]. These techniques are non-destructive and are based on a very simple transition of the pollution from one phase to another. Other water purification processes that are also available, such as biological processes, have been implemented. Although biological oxidation and adsorption are less expensive than other approaches, they are inefficient for the degradation of this type of pollutant; therefore, additional removal processes are required.

Therefore, it is important to look for innovative treatment solutions to tackle this problem. New technologies can be included; for instance, various wastewater treatment technologies are already used to completely destroy the remaining persistent pollutants.

For this purpose, heterogeneous photocatalysis has been identified as a valuable method [7,8] because of its ability to completely remove (mineralize) a wide variety of

organic contaminants with no generation of dangerous intermediate products. Moreover, it has shown the ability to degrade a large variety of organic pollutants. Indeed, it has already been reported by researchers that TiO₂ is a catalyst that gives a high activity due to its large surface area [9,10].

Nevertheless, the semiconductor cannot be easily separated from the treated solution, so a recycling operation is required, which is expensive and difficult to implement on a large scale [11]. Therefore, our goal in this paper was to optimize the efficiency of the catalyst and to not vary its concentration. To examine the stability of TiO₂ for each concentration of the dye, three reusability tests were performed that showed the stability of the catalyst due to the reproducibility of the results [12]. Consequently, cellulose fibers coated with a mixture of catalyst (TiO₂ Millennium PC 500), zeolite, and silica were considered in this study. Table 1 summarizes the different processes used for the photocatalytic treatment of wastewater from the food industry. To the best of our knowledge, there are no detailed studies on the degradation of brilliant blue in recirculating batch and ring reactors using the semiconductor TiO₂ Millennium PC 500, which was the focus of this study.

Table 1. Different processes used for the degradation of wastewater from an agri-food activity.

Process	The Pollutant	References
DBD Plasma Process	Tartrazine	[13]
Electro Fenton	Tartrazine	[14]
Fenton and photo-Fenton	Acid blue 9	[15]
UV/Nano-TiO ₂ Fenton-Like Electro-Fenton and electrocoagulation process	Acid blue 9	[16]
Electro-Fenton	Tartrazine	[17]
Adsorption	Acid blue 9	[18]
Adsorption	Acid blue 9	[19]
Photodegradation using TiO ₂ based Catalysts	Acid blue 9	[20]
Adsorption	Acid blue 9	[21]
Aerobic biodegradation	Acid blue 9	[22]

2. Materials and Methods

2.1. Chemicals

All the chemical reagents used were purchased from Sigma Aldrich, namely FCF Brilliant Blue E133 (Table 2) under the reference code 229730050 and CAS number 3844-45-9, NaCl 99%, Na₂HPO₄ 99%, (HCl 37%), (NaOH, 98%). Stock samples were prepared from high purity water produced by a Millipore Milli-Q system.

2.2. Catalyst and Reactor

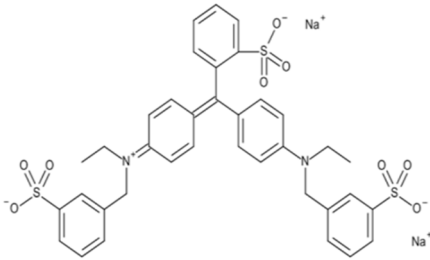
2.2.1. Catalyst

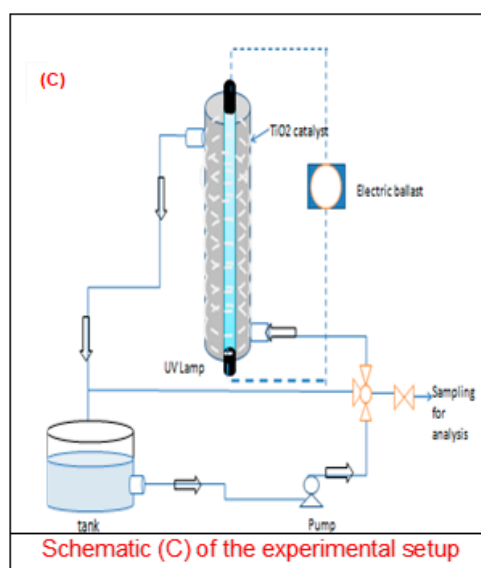
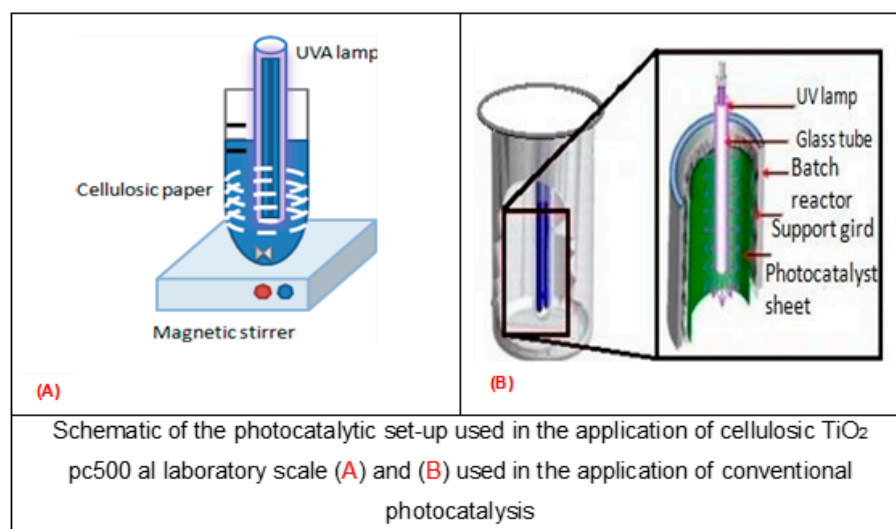
The photocatalytic medium supplied by Ahlstrom Company, under the reference Alhström_1048, was a nonwoven textile composed of cellulose fibers coated with a mixture of catalyst (TiO₂ Millennium PC 500), zeolite, and silica. Their mass per square meter were 16.5, 3.4, and 13.3 g m⁻², respectively. The thickness of the catalyst layer was equal to 250 µm. The median diameter of the pellets deposited on the medium was 1.4 µm.

2.2.2. Batch Reactor

1 L solution of brilliant blue was placed in a reactor (Figure 1A,B) with an UV lamp and a TiO₂ pc 500 photocatalyst supported on a cellulose paper surrounded inside the tank. The solution was covered with aluminum foil to shield it from ultraviolet rays and to improve the light intensity of the tank.

Table 2. Structure and characteristics for the photocatalytic of brilliant blue.

Structure	
Chemicals class	Triphenylmethane
λ_{\max} (nm)	630
M (g/mol)	792.86

**Figure 1.** Photocatalytic montages used during this study.

2.3. Pilot Reactor

The annular recirculation photoreactor (Figure 1C) was composed of two concentric Pyrex tubes, using an 80 W UV light source. The luminous tube was positioned inside the

cylinder. The large tube was 80 cm long and was coated with a photocatalytic medium. The surface area of the catalyst was 0.19 m². The bright blue pollutant passed across the interannular space corresponding with the area shaded in (Figure 1C). In this study, the volume of the bright blue solution was fixed at 4 L, but the concentration of the pollutant was varied. The treatment of water was periodically sampled and analyzed. It is also important to state that the solution was kept in the dark for 20 min to attain adsorption equilibrium before photo-illumination.

Characterization

The morphological analysis of the TiO₂ tissue of cellulosic paper was carried out by scanning electron microscopy (SEM) JEOL JFC-2300HR JEOL JSM-IT 100 with an acceleration voltage of 20 kV.

The absorbance measurements were carried out using a Shimadzu UV-1800 diode array spectrophotometer. Regarding vibrational analyses, they were carried out by Fourier transform infrared spectroscopy (FT/IR-4600).

2.4. Procedure

Conventional photocatalysis experiments were performed using a semiconductor (TiO₂) supported on cellulose paper in a conventional photoreactor with a central 30 W UVA lamp (Phillips PL-L24W/10/4P) with an emission peak at 365 nm; it was placed in a transparent, quartz, crystal tube and immersed in the photoreactor (Figure 1A). A borosilicate glass beaker with a discontinuous scale was used as the reactor for the laboratory experiments. The reactor was filled with 1 L of aqueous solution and different initial concentrations of pollutants at room temperature. A magnetic stirrer was used to circulate and homogenize the medium. To examine the stability of the semiconductor, three cycles were carried out. Each time that the semiconductor was to be reused, it was washed with distilled water and left to dry, so that it could be ensured that the pores were free from the dyes and that, as shown in the degradation results, the catalyst had not lost its photocatalytic properties.

The surface area of the semiconductor used in the pilot scale was three times larger than that used in the laboratory scale. The experiments were performed in a recirculating ring reactor consisting of two concentric Pyrex tubes (Figure 1C), operated in continuous mode, and fed with 4 L of contaminated solution at a flow rate of 200 m³/h to 800 m³/h.

TiO₂ regeneration was performed in ultrapure water under UVA and by shaking after each photocatalytic experiment. The photocatalyst was inserted into the reactor and UV irradiation was delivered by a light source. The solution was kept in the dark before light irradiation to reach an adsorption-desorption equilibrium between the pollutant and the photocatalyst. Aqueous pollutant concentrations were measured at the optimum dye absorption at 630 nm wavelength by a Shimadzu UV-1800 UV-vis spectrophotometer using a quartz cell. The degradation efficiency (%) was predicted using Equation (1):

$$\% \text{Degradation} = \left(\frac{C_0 - C_T}{C_0} \right) \times 100 \quad (1)$$

C₀: Initial concentration of BB.

C_T: Concentration at time t, respectively.

The total organic carbon (TOC) was measured using a TOC analyzer (Shimadzu TOC-VCSH) and the yield rate was calculated according to Equation (2).

$$\% \text{Mineralization} = \frac{\text{TOC}_0 - \text{TOC}_T}{\text{TOC}_0} \times 100 \quad (2)$$

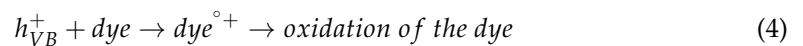
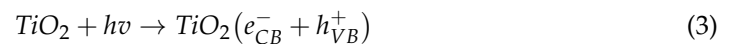
TOC₀: Initial total organic carbon.

TOC_T: Total organic carbon at time t.

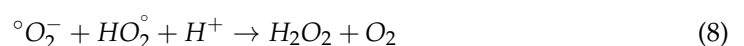
3. Results and Discussion

The impact of several different parameters on the elimination of the bright blue pollutant FCF E133 was tested, specifically pH, initial concentration of the pollutant, and the effect of the addition of inorganic salts. The performances of the geometric configuration of the reactors (laboratory and pilot scale) were also tested and compared, as well as the reuse of the cellulosic paper. The process of degradation was followed by identifying both the decolorization of the pollutant (degradation) and the level of mineralization through spectrophotometry and the total organic carbon determination of the samples taken.

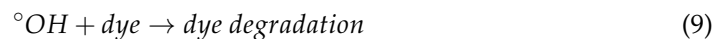
According to the results obtained, there was a degradation rate of 95.7% at a concentration of 10 ppm. Concerning possible photolysis, the observed stability showed that UV alone was not sufficient to degrade the target molecule (Figure 2B) and hence, TiO₂ was necessary. Indeed, it has been shown that the photocatalytic degradation of organic matter in the solution is triggered by the photoexcitation of the semiconductor, with the subsequent creation of an even electron-hole on the catalyst surface (Equation (3)). The high oxidizing potential of the hole (h⁺ VB) in the catalyst allows for the immediate oxidation of organic matter (dye) to reactive intermediates (Equation (4)). Similarly, highly reactive hydroxyl radicals are formed either by the decomposition of water (Equation (5)) or by the reaction of the hole with OH⁻ (Equation (6)). The hydroxyl radical is a highly selective and non-selective oxidant (E⁰ = +3.06 V) that leads to the partial or total mineralization of several organic products.



This radical, in the presence of organic traps, can form organic peroxides (Equation (7)) or hydrogen peroxide (Equation (8))



Conduction electrons are also responsible for producing hydroxyl radicals, which have been designated as the primary cause of mineralization of organic matter (Equation (9)) [23,24].



3.1. Laboratory Scale

3.1.1. Effect of the Pollutant Concentration

Figure 3A illustrates bright blue degradation efficiency using a batch photocatalytic reactor. The experiments were performed with a variance from 5 to 20 mg.L⁻¹ of pollutant. It was found that by increasing the concentration, the removal efficiencies of the pollutant decreased. This can be attributed to the influence of the pollutant input concentration on degradation kinetics, which must be related to the provision of the semiconductor-active sites. Many authors have reported similar results [25,26]. Figure 3B records the concentration impact on mineralization efficiency. As monitored, the 4-fold increase in concentration led to a 27% reduction in total organic carbon. This can be ascribed to the accessibility of free active sites on the catalyst surface (°OH, h⁺, etc.). Indeed, at high

concentrations, the solution is rendered impermeable to UV irradiation, which leads to a poor production of radical hydroxyls and to a diminution of active sites [27].

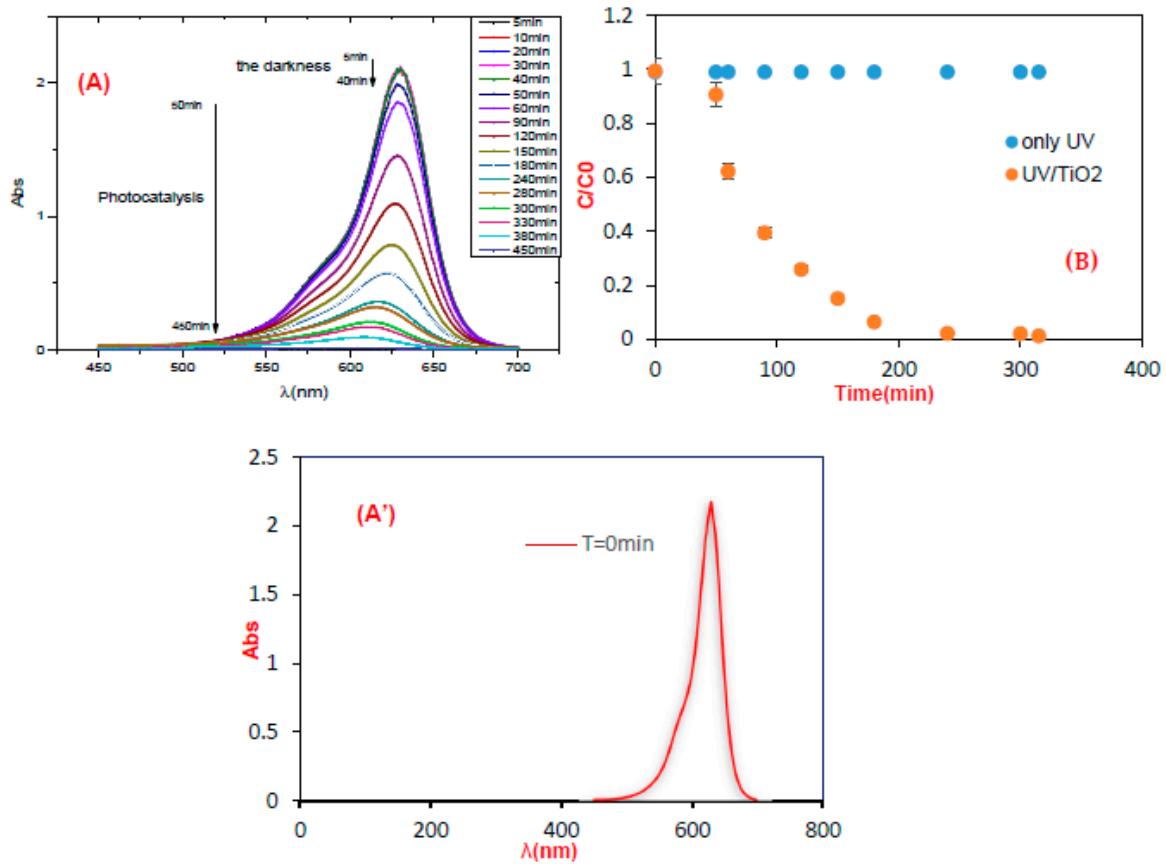


Figure 2. (A) Changes in the UV-Vis spectra of BB FCF E133 (10 ppm) in an aqueous dispersion of TiO₂ (mTiO₂ = 0.3 g) irradiated with a lamp at neutral pH, sometimes: 15 min, 30 min, and 60 min. (A') The standard curve of brilliant blue at t = 0 min (B) Effect of UV light and TiO₂ on the photocatalytic degradation of BB FCF E133. [BB] 0 = 10 ppm, TiO₂ = 0.3 g, pH neutral.

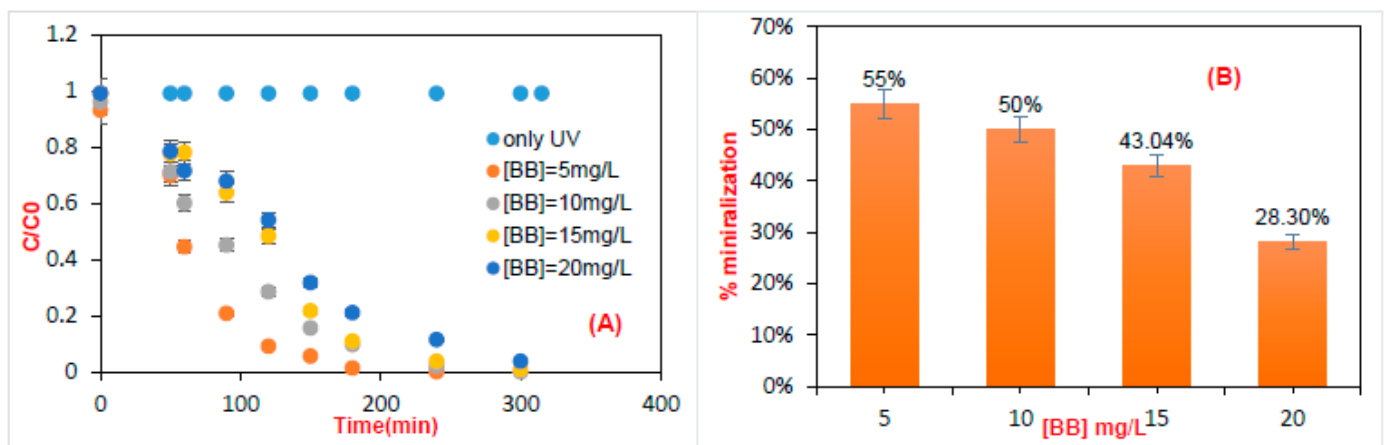


Figure 3. (A) Effect of bright blue concentration on time of UV irradiation. The following test conditions were considered: pH = 6.8 and mTiO₂ = 0.3 g. (B) Photocatalytic mineralization of bright blue with different input concentrations after 5 h of irradiation.

3.1.2. Study of the Catalyst Cycle

The rate of initial degradation of a wide variety of organic materials depends on the concentration of the semiconductor, but our objective in this paper was to optimize the efficiency of the catalyst and to not vary its concentration. To examine the stability of TiO₂ for each dye concentration, three tests were carried out that showed the stability of the catalyst owing to the reproducibility of the results (low error bars) (Figure 3B). This explains why the treated photocatalyst did not lose its photocatalytic properties during the photocatalytic process.

3.1.3. FT-IR Analysis

The FTIR spectra of TiO₂ before and after treatment and brilliant blue are shown in (Figure 4). The wide bands observed at ~3310 cm⁻¹ represent the ν(O-H) group spectrum bands [28]. The bands observed around 2905 cm⁻¹ can be attributed to ν(C-H) vibrations indicating the presence of methylene (-CH₂) and methyl (-CH₃) groups.

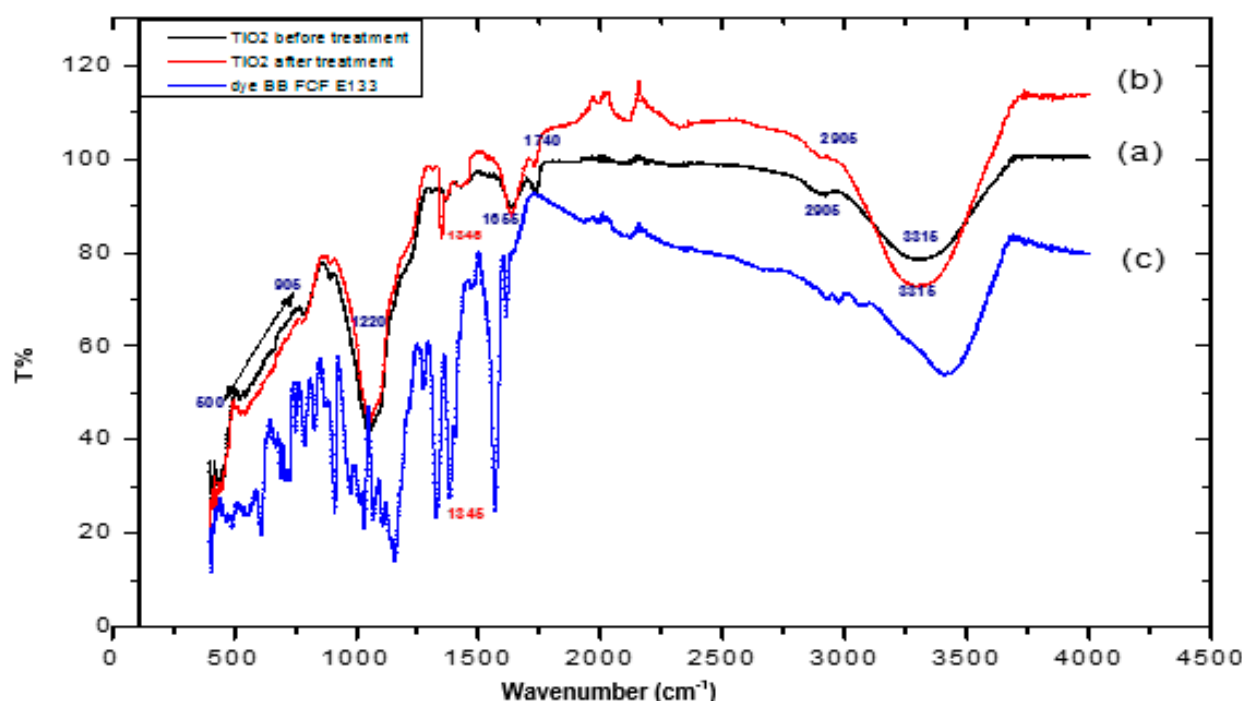


Figure 4. IR spectra of the semiconductor (a) virgin TiO₂, (b) TiO₂ after treatment. (c) Brilliant blue spectrum.

The carbonyl stretches ν (C=O) that have been found at 1740 cm⁻¹ characterize the ester and aldehyde groups [29]. Regarding the carboxyl stretches (COO-) related to secondary and primary alcohols, as well as aliphatic and etheric groups, they were found at 1655 cm⁻¹. The spectral range comprised between 1220 and 1370 cm⁻¹ corresponding with the stretching vibrations of esters (C-O), and the low-intensity bands located between 550 and 900 cm⁻¹ corresponded with Ti-O-Ti vibrations. In addition, it can be noted that in the TiO₂ spectrum after treatment, there was a peak that appeared at 1345 cm⁻¹. According to [18,30], the peak in this area corresponded with a sulfonated group in the dye ring; this new peak confirmed the attachment of dye sulfonate groups to TiO₂ and hence, the adsorption of the pollutant on the semiconductor.

3.1.4. SEM Analysis

Scanning Electron Microscope (SEM) observations were also carried out on the studied semiconductor to evaluate the evolution of the morphology and size of the crystallites. (Figure 5) gathers the images obtained on the TiO₂ supported on a cellulosic paper before

and after photocatalysis. In addition, this study was completed with titanium dioxide supported on a cellulosic paper used in the degradation of food coloring (brilliant blue E133) to see if the presence of this element in the matrix of titanium dioxide on a cellulose paper changed the shape and size of the particles.

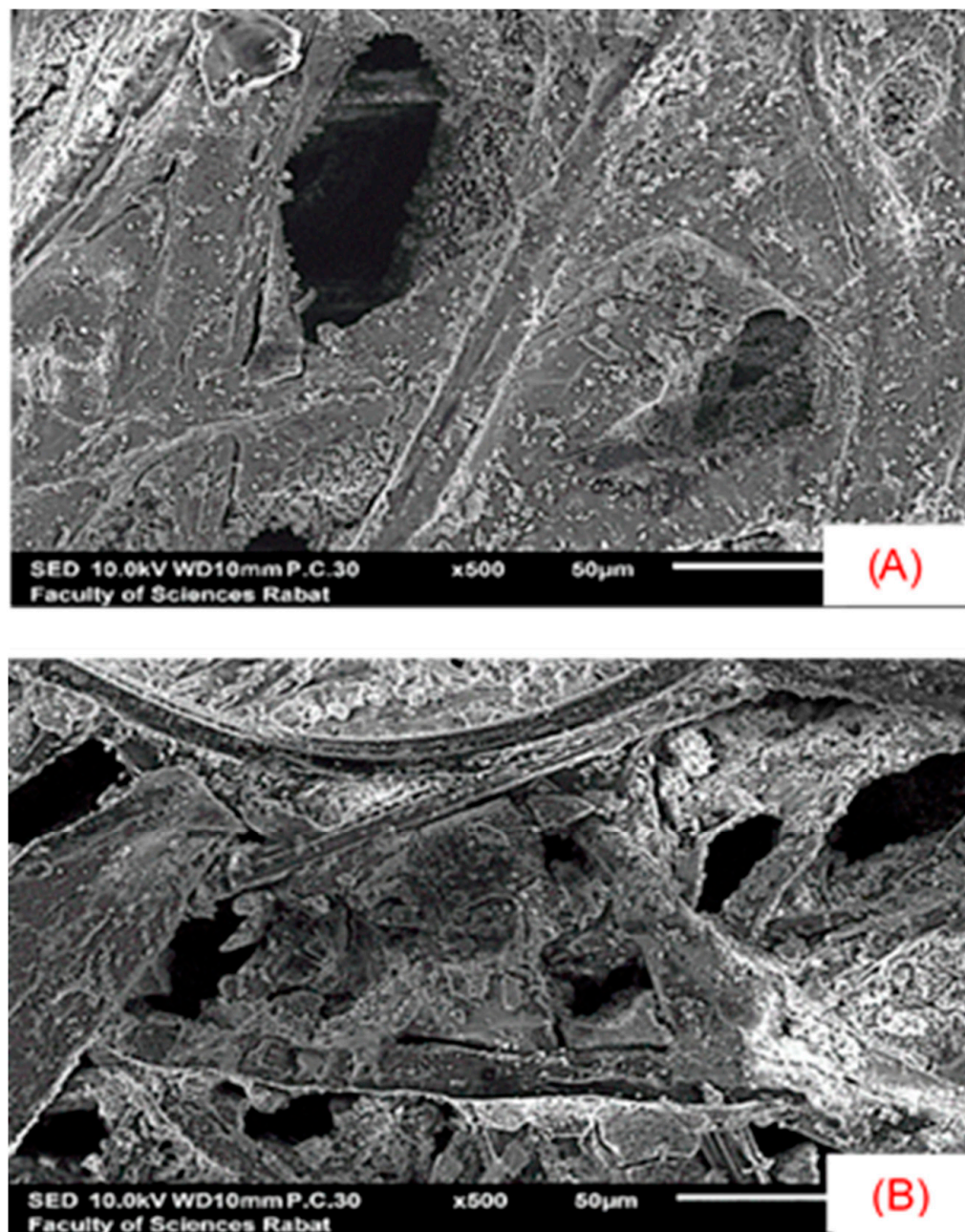


Figure 5. SEM Imaging [(A) before and (B) after photocatalysis].

SEM characterizations were carried out at different magnifications before and after photodegradation of the pollutant. The semiconductor morphology is shown in (Figure 5A,B). A highly porous network (porosity $\approx 82\%$), which can be related to TiO_2 aggregates, was observed in the surface of the cellulose fibers rather than in the pores formed between the fibers.

However, for (Figure 5B), the pores' size became tighter; this explains the availability of the active sites of the semiconductor to the brilliant blue pollutant. The results agree with those of the FT-IR.

3.1.5. Effect of pH

It is necessary to identify the effect of pH on the mineralization and degradation of the targeted pollutant in this process to improve the efficiency of this method. The nature of the TiO_2 catalyst means that any variation in pH could affect the surface charge or isoelectric point of the photocatalyst [31,32]. (Figure 6A) shows that the pH of the zero-point charge (pHpzc) of TiO_2 supported on cellulose paper was 6.9. The effect of pH on the photocatalytic elimination of brilliant blue E133 by TiO_2 under UV irradiation is shown in (Figure 6B), showing the impact of pH on removal efficiency. When the pH was above 6.9, the TiO_2 surface was negatively charged and positively charged below pHpzc. The bright blue was reported to be negatively charged due to SO_3^- groups, making their electrostatic attachment to the TiO_2 surface appropriate in neutral and acidic solutions and not permitted in alkaline media due to the repulsion between the negatively charged TiO_2 surface and organic molecules [33]. As a result, the lowest discoloration was found in alkaline media, while neutral media close to pHpzc appeared to be the most suitable for pollutant degradation (Figure 6B).

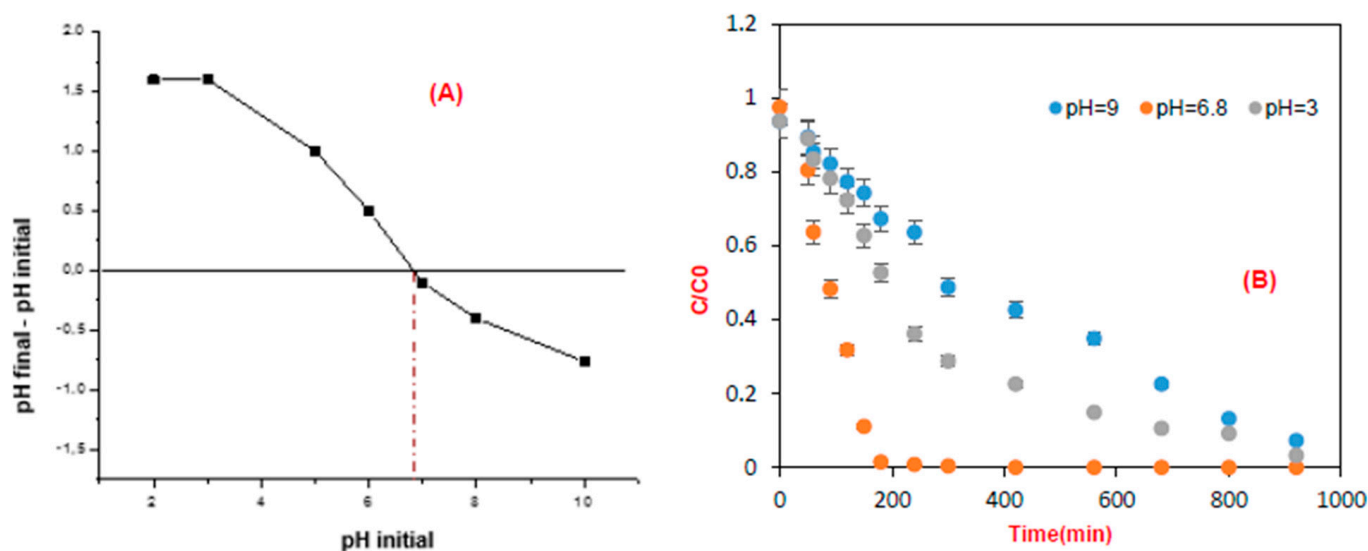


Figure 6. (A) Point of zero charge of TiO_2 , (B) Evolution of the concentration of FCF brilliant blue E133 over time at different pH values.

3.1.6. Effect of the Presence of Salts

In an industrial food processing unit, the properties of the generated wastewater generally reflect the activities carried out. Particularly, the production process is associated with variations that are moderate compared with the activities of cleaning and washing. This is confirmed by the different trends in the different samples taken. The rinsing, cleaning, and washing activities are generally characterized by a higher volume of effluent and greater variations in parameters.

It is interesting to study the effects of NaCl and Na_2HPO_4 present in the discharges, because agri-food wastewater is a mixture of organic and inorganic pollutants; therefore, the bright blue dye could also significantly influence photocatalytic activity.

Degradation was examined at the optimal dye concentration and pH (Figure 7). In the absence of NaCl , the degradation rate was 98% and 50% mineralization, while 37% degradation and 13% mineralization rate were obtained for 80 ppm NaCl . Chloride ions can have an inhibitory effect on the degradation kinetics of brilliant blue, which can be explained by a competition of chloride ions with the pollutant to react with the generated radicals.

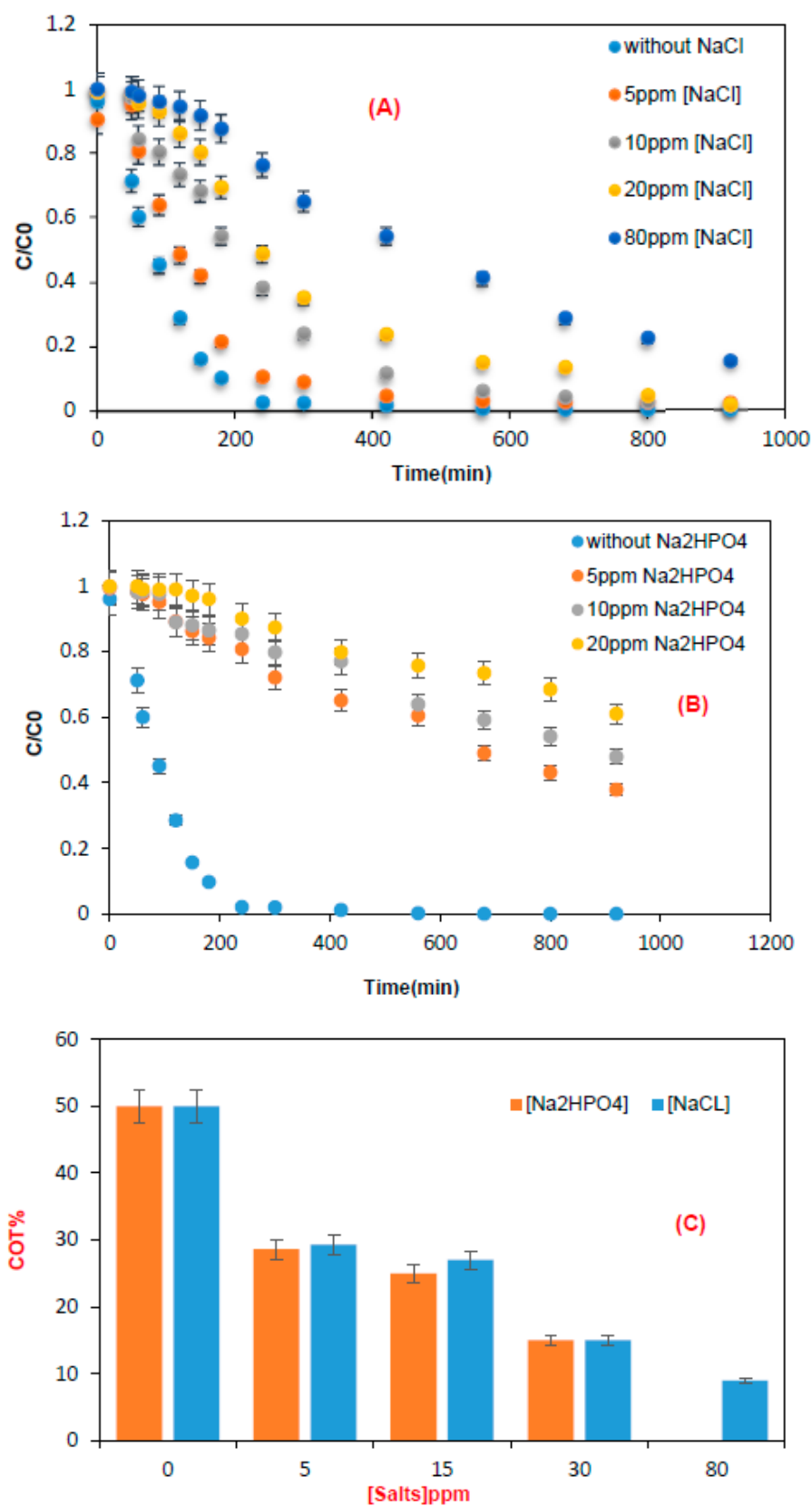


Figure 7. Time-courses of brilliant blue degradation in the presence of (A) NaCl and (B) Na₂HPO₄. (C) Photocatalytic mineralization of brilliant blue in the presence of various concentrations of NaCl and Na₂HPO₄. Experimental conditions: batch reactor, pH = 7, and mTiO₂ = 0.3 g.

For the effect of Na_2HPO_4 addition on the degradation rate, removal efficiency decreased from 98% in the absence of salt to 38.8% for 20 mg of Na_2HPO_4 , respectively. The salt can penetrate the active sites of the TiO_2 surface and thus reduce the rate of degradation of the studied molecule. Moreover, the inhibitory effects of H_2PO_4^- can be explained by the reaction of the hydroxyl radical ($^{\circ}\text{OH}$) and the positive holes (h^+) with these anions (Table 3) [33,34].

Table 3. Characteristics of wastewater from the food industry.

Parametre	Unités	Valeurs		
		Minimum	Moyenne	Maximum
pH	mg/L	5.4	11.7	12.7
Nitrate	mg/L	16.4	17.0	44.0
Sulfure	mg/L	0.0	0.1	0.2
Chlorure	mg/L	22	78	126
Orthophosphate	mg/L	17	34	70

The increase in salt concentration influences degradation and mineralization, having a negative impact on the kinetics and causing the adsorption to become slow. This could be due to the competitive adsorption that exists between the salt ions and target molecule.

3.2. Pilot-Scale

Effects of Inlet Concentration and Flow Rate

The influence of flow rate and pollutant inlet concentration must be clearly defined to determine the performance of photocatalytic oxidation. (Figure 8) shows the efficiency of the recirculating reactor in the degradation and mineralization of brilliant blue [35].

The experiments were carried out, ranging from 200 m^3/h to 800 m^3/h for two different flow rates, and ranging from 10 to 20 mg/L at two concentrations. It can be observed in (Figure 8A,B) that by increasing the flow rate, the efficiency of removal of brilliant blue decreased. This may be due to the decrease of the contact time between the dye and the active sites of TiO_2 . This leads to a small amount of the pollutant being able to react with the active species attached to the catalyst surface. The photocatalytic degradation of the model pollutant decreased remarkably when the input concentration increased [28,36–39]. Indeed, the increase of the amount of dye concentration in the medium limits the efficiency of degradation and mineralization as reported in the literature [40,41].

The equation of the first order kinetic model is of the form:

$$\ln\left(\frac{C_0}{C_t}\right) = K_{\text{app}} \cdot t \quad (10)$$

where:

C_0 : Initial concentration of the pollutant (mg/L).

C_t : Concentration of the pollutant at time t (mg/L).

(Figure 8C) shows the linear regression plot of time vs. $\ln(C/C_0)$ using data presented in (Figure 8A). The curves show that the degradation rate decreased by decreasing the BB concentration [28,36–38,42,43]. Through linear regression, using the plot in (Figure 8C), we found that the pseudo-first order well described the kinetic degradation of BB in the presence of TiO_2 supported on cellulose paper, which is confirmed by the coefficients of correlation presented in Table 4.

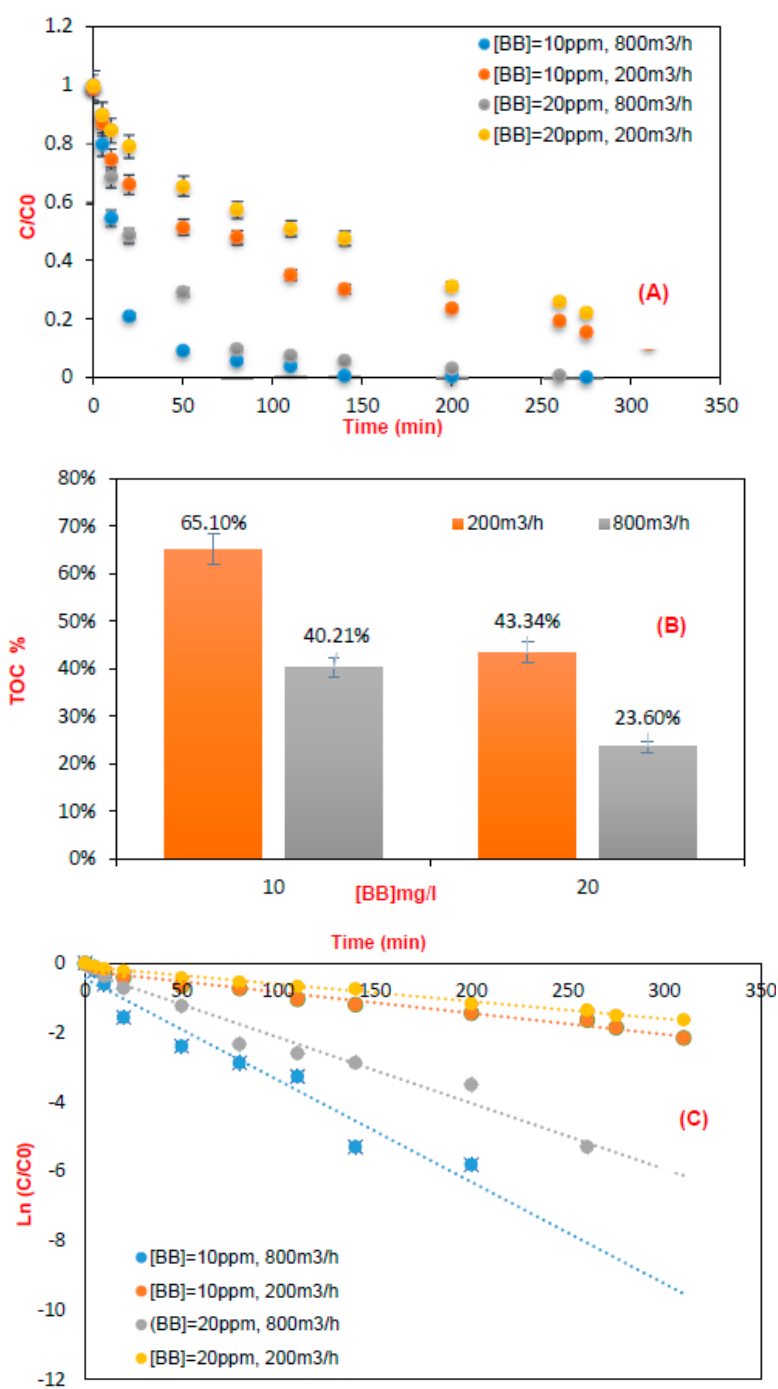


Figure 8. (A) Variation of the bright blue concentration as a function of time (circulation reactor; pH = 6.8 at a flow rate of $Q = 800$ and $200 \text{ m}^3 \cdot \text{h}^{-1}$, [BB] = 10 and 20 ppm), (B) Photocatalytic mineralization with the same conditions. (C) Linear plot of the first order kinetics model.

Table 4. Parameters of first-order kinetics.

Experimental Conditions	$k_{app} \text{ (mg L}^{-1} \text{ min}^{-1}\text{)}$	R^2
[BB] = 10 ppm, $800 \text{ m}^3/\text{h}$	0.0293	0.9478
[BB] = 10 ppm, $200 \text{ m}^3/\text{h}$	0.0061	0.9721
[BB] = 20 ppm, $800 \text{ m}^3/\text{h}$	0.0189	0.9688
[BB] = 20 ppm, $200 \text{ m}^3/\text{h}$	0.005	0.9912

4. Conclusions

Environmental protection is a major problem for humanity. The treatment and reuse of industrial water has become an urgent necessity. Brilliant blue is one of the most used dyes in the food industry, and for this reason, we were interested in the photocatalytic removal of this model pollutant.

In the present work, a parametric study was carried out using a laboratory reactor and a pilot reactor to test the efficiency of photocatalytic degradation of brilliant blue. The influence of pH and initial concentration of the pollutant, as well as the effect of salts, on the efficiency of the removal was studied using the semi-conductor titanium dioxide supported on a cellulose paper which was reused by washing with distilled water, and was characterized by SEM and FTIR before and after proceeding with photodegradation.

Fourier transform infrared spectroscopy (FTIR) showed a new peak that appeared at 1345 cm^{-1} corresponding with a sulfonated group. This new peak confirms the attachment of sulfonate groups of the dye to TiO_2 and thus, the adsorption of the pollutant on the semiconductor.

However, through use of the Scanning Electron Microscope (SEM) after treatment, pore size tightened, which explains the availability of the active sites of the semiconductor by the brilliant blue pollutant.

The following conclusions were drawn:

1. Degradation of the model pollutant was observed in the presence of UV light and the photocatalyst, not in the presence of UV light alone;
2. Maximum degradation of the brilliant blue was observed under neutral conditions, which was explained by catalyst-molecule attractions;
3. For low concentration of brilliant blue, high degradation and mineralization were obtained, which was correlated with the high availability of reactive species;
4. Brilliant blue inlet concentration and flow rate were studied in a pilot-scale recirculation reactor, and it was shown that degradation and mineralization efficiencies decreased at high concentrations due to the decrease in contact time between the pollutant and the catalyst-active sites.

Author Contributions: Conceptualization, F.D.; Methodology, A.A. and A.A.A.; Software, B.R.; Validation, F.D., M.R., S.E.H. and F.F.; Formal analysis, B.R., F.F. and A.A.A.; Investigation, F.D., A.A. and A.A.A.; Resources, B.R. and J.M.; Data curation, M.R., A.A., F.F. and A.A.A.; Writing—original draft, J.M.; Project administration, S.E.H. All authors have read and agreed to the published version of the manuscript.

Funding: This work was supported by the bilateral program CNRS (France) and CNRST (Morocco).

Institutional Review Board Statement: Not applicable.

Informed Consent Statement: Not applicable.

Data Availability Statement: No new data were created or analyzed in this study. Data sharing is not applicable to this article.

Conflicts of Interest: The authors declare no conflict of interest.

References

1. Ghasemzadeh, G.; Momenpour, M.; Omid, F.; Hosseini, M.R.; Ahani, M.; Barzegari, A. Applications of nanomaterials in water treatment and environmental remediation. *Front. Environ. Sci. Eng.* **2014**, *8*, 471–482. [[CrossRef](#)]
2. Liu, L.; Liu, Z.; Bai, H.; Sun, D.D. Concurrent filtration and solar photocatalytic disinfection/degradation using high-performance Ag/TiO₂ nanofiber membrane. *Water Res.* **2012**, *46*, 1101–1112. [[CrossRef](#)] [[PubMed](#)]
3. Bilal, M.; Adeel, M.; Rasheed, T.; Zhao, Y.; Iqbal, H.M.N. Iqbal, Emerging contaminants of high concern and their enzyme-assisted biodegradation—A review. *Environ. Int.* **2019**, *124*, 336–353. [[CrossRef](#)]
4. Singh, T.; Srivastava, N.; Mishra, P.; Bhatiya, A.; Singh, N.L. Application of TiO₂ Nanoparticle in Photocatalytic Degradation of Organic Pollutants. *Mater. Sci. Forum* **2016**, *855*, 20–32. [[CrossRef](#)]
5. Yu, F.; Li, Y.; Han, S.; Ma, J. Adsorptive removal of antibiotics from aqueous solution using carbon materials. *Chemosphere* **2016**, *153*, 365–385. [[CrossRef](#)]

6. Zare, K.; Gupta, V.K.; Moradi, O.; Makhlof, A.S.H.; Sillanpää, M.; Nadagouda, M.N.; Sadegh, H.; Shahryari-Ghoshekandi, R.; Pal, A.; Wang, Z.-J.; et al. A comparative study on the basis of adsorption capacity between CNTs and activated carbon as adsorbents for removal of noxious synthetic dyes: A review. *J. Nanostructure Chem.* **2015**, *5*, 227–236. [[CrossRef](#)]
7. Gan, Y.; Wei, Y.; Xiong, J.; Cheng, G. Impact of post-processing modes of precursor on adsorption and photocatalytic capability of mesoporous TiO₂ nanocrystallite aggregates towards ciprofloxacin removal. *Chem. Eng. J.* **2018**, *349*, 1–16. [[CrossRef](#)]
8. Zhang, M.; Xiong, J.; Yang, H.; Wen, Z.; Chen, R.; Cheng, G. Surface potential/wettability and interface charge transfer engineering of copper-oxides (Cu-MOx, M = W, Ti, and Ce) hybrids for efficient wastewater treatment through adsorption-photocatalysis synergy. *Ind. Eng. Chem. Res.* **2020**, *59*, 15454–15463. [[CrossRef](#)]
9. Patchaiyappan, S.; Saran, S.P. Devipriya Recovery and reuse of TiO₂ photocatalyst from aqueous suspension using plant based coagulant—A green approach Korean. *J. Chem. Eng.* **2016**, *33*, 2107–2113.
10. Qiu, P.; Lu, M.; Cheng, G.; Li, W.; Liu, L.; Xiong, J. Co-implantation of oxygen vacancy and well-dispersed Cu cocatalyst into TiO₂ nanoparticles for promoting solar-to-hydrogen evolution. *Int. J. Hydrogen Energy* **2023**, *48*, 933–942. [[CrossRef](#)]
11. Samhaber, W.M.; Nguyen, M.T. Applicability and costs of nanofiltration in combination with photocatalysis for the treatment of dye house effluents. *Beilstein J. Nanotechnol.* **2014**, *5*, 476–484. [[CrossRef](#)] [[PubMed](#)]
12. Westerhoff, P.; Alvarez, P.; Li, Q.; Gardea-Torresdey, J.; Zimmerman, J. Zimmerman Overcoming implementation barriers for nanotechnology in drinking water treatment. *Environ. Sci. Nano* **2016**, *6*, 1241–1253. [[CrossRef](#)]
13. Ghezzar, M.R.; Ognier, S.; Cavadias, S.; Abdelmalek, F.; Addou, A. DBDplate-TiO₂ treatment of Yellow Tartrazine azo dye solution in falling film. *Sep. Purif. Technol.* **2013**, *104*, 250–255. [[CrossRef](#)]
14. Ren, G.; Zhou, M.; Liu, M.; Ma, L.; Yang, H. A novel vertical-flow electro-Fenton reactor for organic wastewater treatment. *Chem. Eng. J.* **2016**, *298*, 55–67. [[CrossRef](#)]
15. Qiu, M.; Huang, C. A comparative study of degradation of the azo dye C.I. Acid Blue 9 by Fenton and photo-Fenton oxidation. *Desalination Water Treat.* **2010**, *24*, 273–277. [[CrossRef](#)]
16. Khataee, A.; Vatanpour, V.; Ghadim, A.A. Decolorization of C.I. Acid Blue 9 solution by UV/Nano-TiO₂, Fenton, Fenton-like, electro-Fenton and electrocoagulation processes: A comparative study. *J. Hazard. Mater.* **2009**, *161*, 1225–1233. [[CrossRef](#)]
17. Zhang, C.; Ren, G.; Wang, W.; Yu, X.; Yu, F.; Zhang, Q.; Zhou, M. A new type of continuous-flow heterogeneous electro-Fenton reactor for Tartrazine degradation. *Sep. Purif. Technol.* **2018**, *208*, 76–82. [[CrossRef](#)]
18. Dotto, G.; Pinto, L. Adsorption of food dyes acid blue 9 and food yellow 3 onto chitosan: Stirring rate effect in kinetics and mechanism. *J. Hazard. Mater.* **2011**, *187*, 164–170. [[CrossRef](#)]
19. Yang, R.; Liu, G.; Xu, X.; Li, M.; Zhang, J.; Hao, X. Surface texture, chemistry and adsorption properties of acid blue 9 of hemp (*Cannabis sativa* L.) bast-based activated carbon fibers prepared by phosphoric acid activation. *Biomass Bioenergy* **2011**, *35*, 437–445. [[CrossRef](#)]
20. Caudillo-Flores, U.; Muñoz-Batista, M.J.; Kubacka, A.; Zárate-Medina, J.; Cortés, J.A.; Fernández-García, M. Measuring and interpreting quantum efficiency of acid blue 9 photodegradation using TiO₂-based catalysts. *Appl. Catal. A Gen.* **2018**, *550*, 38–47. [[CrossRef](#)]
21. Ben Torkia, Y.; Atrous, M.; Bouzid, M.; Dotto, G.L.; Ben Lamine, A. Stereographic and energetic studies of acid blue 9 adsorption onto *Spirulina platensis* (strain LEB-52) based on statistical physics approach. *Chem. Eng. Commun.* **2019**, *207*, 445–457. [[CrossRef](#)]
22. Neetha, J.; Ujwal, P.; Sandesh, K.; Santhosh, H.; Girish, K. Aerobic biodegradation of Acid Blue-9 dye by *Bacillus fermus* Isolated from *Annona reticulata*. *Environ. Technol. Innov.* **2018**, *11*, 253–261. [[CrossRef](#)]
23. Marci, G.; Augugliaro, V.; Munoz, M.J.L.; Martin, C.; Palmisano, L.; Schiavello, M.; Tilley, R.J.D.; Venezia, A.M.J. Preparation Characterization and Photocatalytic Activity of Polycrystalline ZnO/TiO₂ Systems. 2. Surface, Bulk Characterization, and 4-Nitrophenol Photodegradation in Liquid–Solid Regime. *Phys. Chem. B* **2001**, *105*, 1033.
24. Galindo, C.; Jacques, P.; Kalt, A.J. Photodegradation of the aminoazobenzene acid orange 52 by three advanced oxidation processes: UV/H₂O₂, UV/TiO₂ and VIS/TiO₂. *Photochem. Photobiol. A* **2000**, *130*, 35–47. [[CrossRef](#)]
25. Merabet, S.; Assadi, A.A.; Bouzaza, A.; Wolbert, D. Photocatalytic degradation of indole-4-methylphenol mixture in an aqueous-solution: Optimization and statistical analysis. *Desalin. Water Treat.* **2016**, *57*, 17039–17050.
26. Carp, O.; Huisman, C.L.; Reller, A. Photoinduced reactivity of titanium dioxide. *Prog. Solid State. Chem.* **2004**, *32*, 33–177. [[CrossRef](#)]
27. Bharati, R.; Suresh, S. Biosynthesis of ZnO/SiO₂ nanocatalyst with palash leaves' powder for treatment of petroleum refinery effluent. *Reffit* **2017**, *3*, 528–541. [[CrossRef](#)]
28. Azzaz, A.A.; Assadi, A.A.; Bouzaza, B.; Wolbert, D.; Rtimi, S.; Bousselmi, L.; Jellali, S. Discoloration of simulated textile effluent in continuous photoreactor using immobilized titanium dioxide: Effect of zinc and sodium chloride. *J. Photochem. Photobiol. A Chem.* **2018**, *358*, 111–120. [[CrossRef](#)]
29. Rabahi, A.; Assadi, A.A.; Nasrallah, N.; Bouzaza, A.; Maachi, R.; Wolbert, D. Photocatalytic treatment of petroleum industry wastewater using recirculating annular reactor: Comparison of experimental and modeling. *Environ. Sci. Pollut. Res.* **2018**, *26*, 19035–19046. [[CrossRef](#)]
30. Sakkayawong, N.; Thiravetyan, P.; Nakbanpote, W. Adsorption mechanism of synthetic reactive dye wastewater by chitosan. *J. Hazard. Mater.* **2011**, *187*, 164–170.

31. N'guettia, R.K.; Gombert, B.; Soro, B.-D.; Traore, S.K.; Vel Leitner Karpel, N. Photocatalytic degradation of 5-fluorouracil by a UV-A/TiO₂ system: Effect of catalyst and pollutant concentration, pH and dilution matrices. *Int. J. Biol. Chem. Sci.* **2017**, *11*, 1373. [[CrossRef](#)]
32. Aljuboury D al Deen, A.; Al-Abri, M.; Shaik, F.; Al-Sabahi, J.N.; Alkhadori, A.N. Assessment of TiO₂/ZnO/H₂O₂ Photocatalyst to treat wastewater from oil refinery within visible light circumstances. *South Afr. J. Chem. Eng.* **2020**, *35*, 69–77. [[CrossRef](#)]
33. Shahrezaei, F.; Mansouri, Y.; Zinatizadeh, A.A.L.; Akhbari, A. Process modeling and kinetic evaluation of petroleum refinery wastewater treatment in a photocatalytic reactor using TiO₂ nanoparticles. *Powder Technol.* **2012**, *221*, 203–212. [[CrossRef](#)]
34. Hu, C.; Yuchao, T.; Lanyu, L.; Zhengping, H.; Yizhong, W.; Hongxiao, T. Effects of inorganic anions on photoactivity of various photocatalysts under different conditions. *J. Chem. Technol. Biotechnol.* **2004**, *79*, 247–252. [[CrossRef](#)]
35. Hu, C.; Yu, J.C.; Hao, Z.; Wong, P. Effects of acidity and inorganic ions on the photocatalytic degradation of different azo dyes. *Appl. Catal. B Environ.* **2003**, *46*, 35–47. [[CrossRef](#)]
36. Madriz, L.; Tatá, J.; Carvajal, D.; Núñez, O.; Scharifker, B.; Mostany, J.; Borrás, C.; Cabrerizo, F.M.; Vargas, R. Photocatalysis and photoelectrochemical glucose oxidation on Bi₂WO₆: Conditions for the concomitant H₂ production. *Renew. Energy* **2020**, *152*, 974–983. [[CrossRef](#)]
37. Baaloudj, O.; Nasrallah, N.; Kebir, M.; Guedioura, B.; Amrane, A.; Nguyen-Tri, P.; Nanda, S.; Assadi, A.A. Artificial neural network modeling of cefixime photodegradation by synthesized CoBi₂O₄ nanoparticles. *Environ. Sci. Pollut. Res.* **2020**, *28*, 15436–15452. [[CrossRef](#)]
38. Baaloudj, O.; Nasrallah, N.; Bouallouche, R.; Kenfoud, H.; Khezami, L.; Assadi, A.A. High efficient Cefixime removal from water by the sillenite Bi₁₂TiO₂₀: Photocatalytic mechanism and degradation pathway. *J. Clean. Prod.* **2021**, *330*, 129934. [[CrossRef](#)]
39. Kenfoud, H.; Baaloudj, O.; Nasrallah, N.; Bagtache, R.; Assadi, A.A.; Trari, M. Structural and electrochemical characterizations of Bi₁₂CoO₂₀ sillenite crystals: Degradation and reduction of organic and inorganic pollutants. *J. Mater. Sci. Mater. Electron.* **2021**, *32*, 16411–16420. [[CrossRef](#)]
40. Saoud, W.A.; Assadi, A.A.; Guiza, M.; Bouzaza, A.; Aboussaoud, W.; Ouederni, A.; Soutrel, I.; Wolbert, D.; Rtimi, S. Study of synergetic effect, catalytic poisoning and regeneration using dielectric barrier discharge and photocatalysis in a continuous reactor: Abatement of pollutants in air mixture system. *Appl. Catal. B Environ.* **2017**, *213*, 53–61. [[CrossRef](#)]
41. Zhong, L.; Brancho, J.J.; Batterman, S.; Bartlett, B.M.; Godwin, C. Experimental and modeling study of visible light responsive photocatalytic oxidation (PCO) materials for toluene degradation. *Appl. Catal. B Environ.* **2017**, *216*, 122–132. [[CrossRef](#)] [[PubMed](#)]
42. Vargas, R.; Núñez, O. Photocatalytic degradation of oil industry hydrocarbons models at laboratory and at pilot-plant scale. *Sol. Energy* **2010**, *84*, 345–351. [[CrossRef](#)]
43. Liu, B.; Zhao, X.; Terashima, C.; Fujishima, A.; Nakata, K. Thermodynamic and kinetic analysis of heterogeneous photocatalysis for semiconductor systems. *Phys. Chem. Chem. Phys.* **2014**, *16*, 8751–8760. [[CrossRef](#)] [[PubMed](#)]

Disclaimer/Publisher's Note: The statements, opinions and data contained in all publications are solely those of the individual author(s) and contributor(s) and not of MDPI and/or the editor(s). MDPI and/or the editor(s) disclaim responsibility for any injury to people or property resulting from any ideas, methods, instructions or products referred to in the content.